Direct-Drive Irradiation Uniformity for the NIF

The National Ignition Facility (NIF) can have the flexibility to perform direct-drive experiments, in addition to indirect drive, if two key elements are included in its design: (1) The facility must be able to redirect 24 of the beam clusters to new beam ports near the "equator" of the target chamber, and (2) two-dimensional smoothing by spectral dispersion[1] (2-D SSD) must be implemented.

In this article, we first address how the indirect-drive irradiation geometry must be modified to accommodate direct drive. Emphasis is placed on finding an acceptable direct-drive geometry that minimizes the amount of reconfiguration. Tolerances for energy imbalance, beam mispointing, and target-positioning errors are discussed for the proposed irradiation geometry. The beam uniformity that can be achieved using 2-D SSD is also examined. One related laser design issue that affects the level of uniformity is pinhole size. The pinholes determine the maximum amount of angular spectral dispersion that can be used with SSD. The dependence of uniformity on pinhole size is discussed. Finally, the SSD-smoothed beam profile is combined with the direct-drive beam geometry to calculate the irradiation uniformity on a spherical target with multiple overlapping beams.

Beam Placement

Because the NIF will have only a single target chamber (designed primarily for indirect drive), a direct-drive component must be integrated into the system without major modifications. The current design for beam placement at the NIF target chamber, given in Table 62.I, has 48 beams in eight latitudinal rings clustered near the poles. Each beam consists of a cluster of four beamlets, separated in wavelength by about 5 Å. Such an irradiation scheme, taken as a whole, does not lend itself to direct drive. However, a portion of the beam positions would be suitable if additional beam ports were added near the equator. Such configurations have been considered by Mark,[2] who pointed out that direct-drive beams need not be uniformly disposed but could be placed in rings at polar angles given by the zeros of a Legendre polynomial. However, in general, the beams from different rings must have different energies, corresponding to the weights of Gaussian quadrature. One such configuration, which closely meshes with the current NIF design, is based on rings of beams at the zeros of the P_6 Legendre polynomial, with polar angles given by $\theta = 21.17°$, 48.60°, 76.19°, 103.81°, 131.40°, and 158.83°. Examination of the beam-port positions in Table 62.I shows that four of the rings in that design correspond very well to four of these angles, namely the ports at 23.49°, 48.27°, 131.73°, and 156.73°. For half of the beam ports, no modification would be required (except possibly for a small pointing correction so that the beam axes pass through the target surface, closer to the required latitudes). The remaining 24 beam clusters would have to be redirected into new beam ports positioned at 76.19° and 103.80° (Table 62.II).

The number of beam clusters in each ring for this direct-drive configuration is 4, 8, and 12 for the upper hemisphere, and similarly for the lower. The laser energies coming from each of these rings must be in the proportion of 1 to 2.105 to 2.731. Distributing this energy among the beams in each ring, we find that the relative energies for beams from different rings are 0.95, 1.00, and 0.86, which implies that beams from the polar and equatorial rings must be reduced in energy relative to beams from the ring at $\theta = 48°$. The net result is that ~8% of the available laser energy cannot be used for target irradiation, which represents a relatively small energy penalty for the flexibility of adding a direct-drive option to the current NIF design.

The irradiation uniformity for this 48-cluster configuration is shown in Fig. 62.21. The rms nonuniformity is plotted as a function of how much the beam overfills the target, for a smooth eighth-order supergaussian beam profile. (The edge of the beam was defined as the 5% intensity contour.) The nonuniformity is entirely long-wavelength structure, characterized by how well the 48 overlapping clusters of beams can cover a sphere. (The effect of short-wavelength nonuniformity from structure on the individual beams is examined in the next section.) For conditions at the onset of irradiation, the beam-to-target ratio should be chosen to be about 1.1. As the target implodes, this ratio becomes larger, and the long-wavelength

Table 62.I: NIF beamport assignments — indirect drive

Port #	θ	ϕ	Port #	θ	ϕ
n01	23.4895	78.750	n25	123.3311	5.625
n02	23.4895	168.750	n26	123.3311	50.625
n03	23.4895	258.750	n27	123.3311	95.625
n04	23.4895	348.750	n28	123.3311	140.625
n05	31.9844	33.750	n29	123.3311	185.625
n06	31.9844	123.750	n30	123.3311	230.625
n07	31.9844	213.750	n31	123.3311	275.625
n08	31.9844	303.750	n32	123.3311	320.625
n09	48.2682	16.875	n33	131.7317	28.125
n10	48.2682	61.875	n34	131.7317	73.125
n11	48.2682	106.875	n35	131.7317	118.125
n12	48.2682	151.875	n36	131.7317	163.125
n13	48.2682	196.875	n37	131.7317	208.125
n14	48.2682	241.875	n38	131.7317	253.125
n15	48.2682	286.875	n39	131.7317	298.125
n16	48.2682	331.875	n40	131.7317	343.125
n17	56.6688	39.375	n41	148.1055	56.250
n18	56.6688	84.375	n42	148.1055	146.250
n19	56.6688	129.375	n43	148.1055	236.250
n20	56.6688	174.375	n44	148.1055	326.250
n21	56.6688	219.375	n45	156.7317	11.250
n22	56.6688	264.375	n46	156.7317	101.250
n23	56.6688	309.375	n47	156.7317	191.250
n24	56.6688	354.375	n48	156.7317	281.250

nonuniformity degrades slightly. The solid line in Fig. 62.21 is the result of pointing the polar ring of beams to the correct latitude on the target surface; the dashed line is without this correction. The effect of the beam-pointing correction is to reduce this contribution to nonuniformity by 30% to 50%.

The effect on uniformity produced by energy imbalance among the beams is shown in Fig. 62.22. (The energy fluctuations among beams within a cluster were assumed uncorrelated.) Conditions with the same rms variation in energy can produce a relatively large spread in nonuniformity, as indicated by the bars in the figure, but it is all very-long-wavelength structure, corresponding to spherical harmonic modes 1 through 4. Similar results were obtained for cluster pointing errors (Fig. 62.23). Target positioning errors, shown in Fig. 62.24, predominantly affect only the mode $\ell = 1$. Generally, the combined contributions from these factors will add harmonically. These factors will make less than a 1% contribution to nonuniformity if the energy imbalance is less than ~5%, cluster pointing is better than 5% of the target radius, and target positioning errors are less than about 2% of the target radius.

The 8% reduction in laser energy can be avoided if the beamports for indirect drive can be shifted by a few degrees

Table 62.II: NIF beamport assignments — direct drive

Port #	θ	ϕ	Port #	θ	ϕ
n01	23.4895	78.750	n25	103.8000	15.000
n02	23.4895	168.750	n26	103.8000	45.000
n03	23.4895	258.750	n27	103.8000	75.000
n04	23.4895	348.750	n28	103.8000	105.000
n05	48.2682	16.875	n29	103.8000	135.000
n06	48.2682	61.875	n30	103.8000	165.000
n07	48.2682	106.875	n31	103.8000	195.000
n08	48.2682	151.875	n32	103.8000	225.000
n09	48.2682	196.875	n33	103.8000	255.000
n10	48.2682	241.875	n34	103.8000	285.000
n11	48.2682	286.875	n35	103.8000	315.000
n12	48.2682	331.875	n36	103.8000	345.000
n13	76.1900	0.000	n37	131.7317	28.125
n14	76.1900	30.000	n38	131.7317	73.125
n15	76.1900	60.000	n39	131.7317	118.125
n16	76.1900	90.000	n40	131.7317	163.125
n17	76.1900	120.000	n41	131.7317	208.125
n18	76.1900	150.000	n42	131.7317	253.125
n19	76.1900	180.000	n43	131.7317	298.125
n20	76.1900	210.000	n44	131.7317	343.125
n21	76.1900	240.000	n45	156.7317	11.250
n22	76.1900	270.000	n46	156.7317	101.250
n23	76.1900	300.000	n47	156.7317	191.250
n24	76.1900	330.000	n48	156.7317	281.250

without affecting indirect-drive target performance. One possibility[3] is to move the rings at 23.49° and 48.27° to new positions at 21.00° and 46.50°. The additional ring of 12 beams, in the upper hemisphere, would be placed at 75.75° rather than 76.19°. The rings in the lower hemisphere would be at 104.25°, 133.50°, and 159.00°. The direct-drive uniformity for this configuration is similar to the solid curve in Fig. 62.21, but with all beam axes now passing through the center of the target. The uniformity requirement for direct drive can be met by either configuration. Clearly, options requiring no energy reduction are preferred.

Beam Smoothing by Spectral Dispersion (SSD)

This section examines issues related to beam smoothing by spectral dispersion (SSD). The starting point for the calculations presented here is the SSD configuration proposed for the NIF by D. Eimerl[4] during the ICFAC meeting at the University of Rochester on 18 May 1994. A key design issue for the NIF that affects optimization of SSD is the angular acceptance of the pinholes, which determines the amount of spectral dispersion that can be used by SSD. It will be shown below that if twice the dispersion specified by Eimerl is imposed (in just one dimension), then a substantial improvement in uniformity can be achieved.

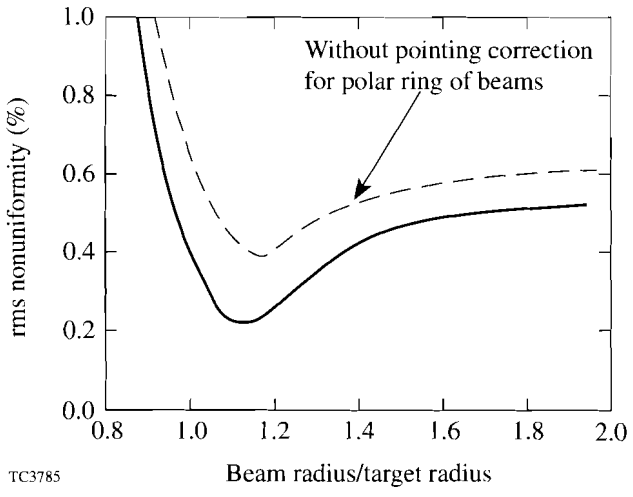

Figure 62.21
The rms nonuniformity for the 48-beam configuration as a function of the ratio of beam size to target size. An eighth-order supergaussian beam profile was used. (The effect of structure on the beams is shown in Fig. 62.29.) The solid line is the result of pointing the polar ring of beams to the optimal position on the target surface. The dashed line is without this correction.

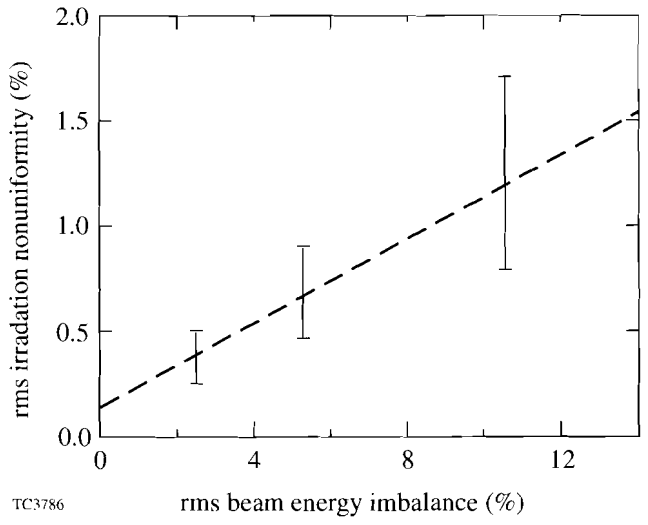

Figure 62.22
The rms irradiation nonuniformity as a function of the rms energy imbalance among the beams. The bars show the spread in irradiation nonuniformity that can occur for a given energy imbalance. Energy fluctuations among beams in a cluster were assumed to be uncorrelated.

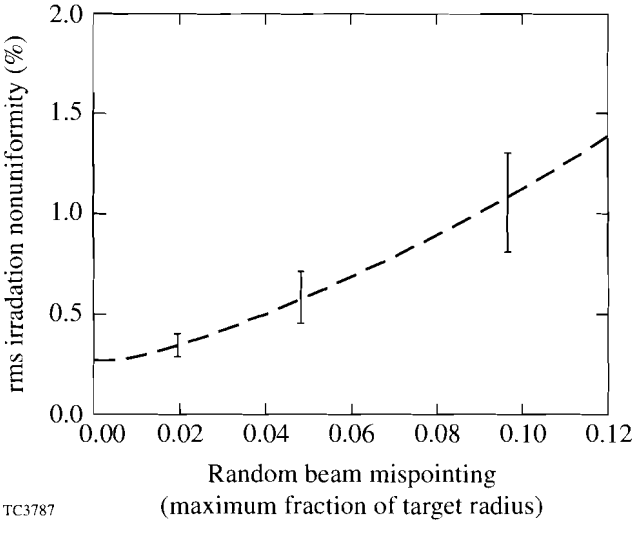

Figure 62.23
The rms irradiation nonuniformity as a function of cluster pointing error. All beams within a cluster were assumed to be pointed in the same direction.

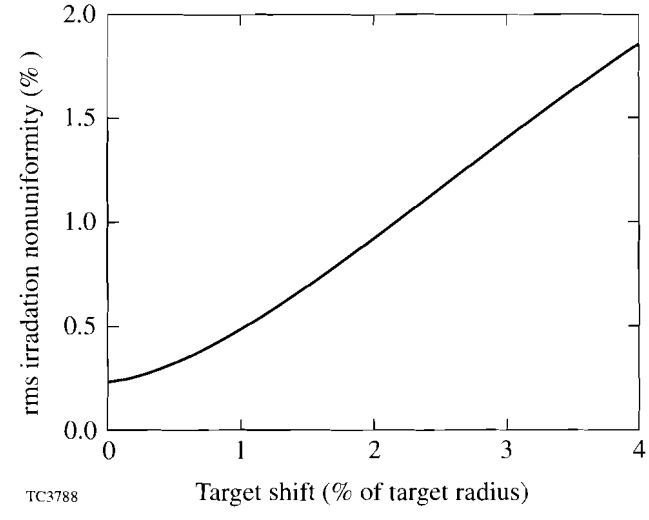

Figure 62.24
The rms irradiation nonuniformity as a function of target positioning error.

The three sets of parameters that determine the single-beam uniformity achievable by SSD are those related to the phase plate, the polarization rotator (or shifter), and the spectrally dispersed bandwidth. The first two parameter sets will be mentioned only briefly as any adjustable parameters associated with them will affect mainly long-wavelength nonuniformities. The third parameter set will be discussed in more detail since this provides the primary smoothing mechanism for short-wavelength structure in the beam and a large number of options are available.

1. Phase Plate

The calculations presented here use a binary phase plate with an array of 250 × 250 square elements, which produces a sinc^2 intensity envelope in the target plane. Superimposed upon this envelope is highly modulated speckle from the interference between rays from different phase-plate elements. Most of this structure is smoothed out by SSD. The distance D between the first zeros of the envelope is equal to 250 times the beam's diffraction limit (for the phase plate considered), i.e.,

$$D = 250 \times \left(2\lambda F^{\#}\right).$$

For an f-number ($F^{\#}$) of 17.5 and $\lambda = 0.35$ mm, we have $D =$ 3 mm, which should correspond to the diameter of the target. Current direct-drive designs for the NIF use targets about 30% larger, which would require a larger number of phase-plate elements (i.e., ~350 × 350 for the above example). More phase-plate elements (of smaller size) would produce a small shift in nonuniformity to shorter wavelengths relative to the target size, but the shift would not be large enough to significantly affect the results presented in the next section.

Current phase-plate strategies involve the use of continuously varying phases[5] and kinoforms[6] to avoid the energy loss around the target associated with the sharp variations in binary phase plates. These will also provide greater control over the shape of the intensity envelope in the target plane. It remains to be determined what effect these new phase plates will have on short-wavelength nonuniformities. They can significantly affect long-wavelength structures (spherical harmonic modes $\ell < 20$) through the envelope shape. (It should be emphasized that any phase-plate envelope shape will be slightly modified by SSD and polarization dispersion.) As target designs and phase-plate strategies develop, their characteristic features can be incorporated into the uniformity calculations to determine their effects.

2. Polarization Dispersion

A birefringent wedge placed at the end of each beamline will cause the speckle pattern from one polarization to shift relative to the other.[7] If the shift is more than about 1/2 of a speckle width (which is roughly the coherence length), then the effect is similar to adding two different random-intensity patterns.[8] The rms nonuniformity will be reduced instantaneously by a factor of $\sqrt{2}$. This effect was demonstrated at LLE using a liquid crystal (LC) wedge,[7] but any other birefringent material, such as KDP, could be used. Figure 62.25 shows the experimental results of how the speckle modulation from a phase plate has been reduced using the LC wedge. An analysis of the intensity fluctuations around a smooth envelope

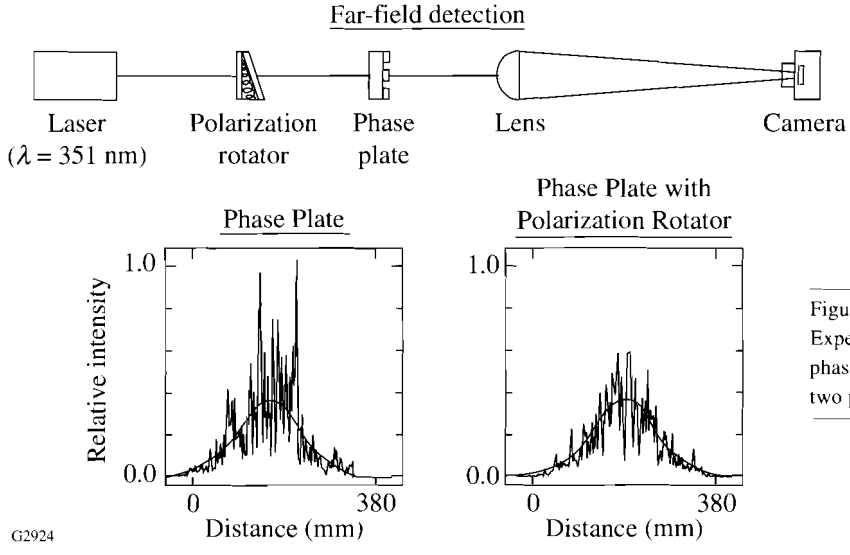

Figure 62.25
Experimentally observed reduction in nonuniformity from a phase plate using a birefringent wedge to spatially separate the two polarization components.

showed that the rms variation was reduced by roughly a $\sqrt{2}$, as predicted. This superposition of shifted speckle patterns is similar to the smoothing mechanism produced by SSD, which shifts the speckle patterns for different spectral modes of the bandwidth. Optimized smoothing is achieved when the polarization and spectral shifts are complementary, as discussed below.

3. SSD Considerations

As the baseline configuration for 2-D SSD, we adopt the parameters described by Eimerl (Fig. 62.26). The one departure from that design, examined here, is the option for increased angular dispersion in one of the directions. It remains to be determined what effect such increased dispersion would have on laser performance and whether the amount of improved laser uniformity is large enough to justify a possible degradation in energy output.

One strategy for combining two-dimensional spectral dispersion of the bandwidth with polarization dispersion from a birefringent wedge is illustrated in Fig. 62.27, which shows the modal positions in the target plane. The minimum separation between modes should not be closer than ~1/2 the diffraction limit of the beam (i.e., 1/2 a speckle size) for good smoothing. The symbols "x" and "o" represent orthogonal components of polarization. This configuration allows for the smallest amount of angular dispersion through the laser but requires the maximum polarization dispersion. To keep the beam nearly circular, either twice as many modes must be used in the direction perpendicular to polarization dispersion (i.e., twice the angular spread) or the beam envelope must be adjusted using the phase plate to compensate for unequal angular dispersion.[1]

To examine the effect of increasing the angular dispersion in one direction, we considered the example where the parameters associated with the 3-GHz modulator (Fig. 62.26) were kept constant and parameters of the other modulator were varied. The 1-Å IR bandwidth from the 3-GHz modulator produces about 31 spectral lines upon frequency tripling. These lines were spectrally dispersed to a separation of 1/2 a speckle distance in the target plane, i.e., a total angular spread of 15 times the beam's diffraction limit (to be denoted by 15 × DL). This was chosen to be the direction of polarization dispersion, which was also 15 × DL, corresponding to the horizontal direction in Fig. 62.27. The total angular deflection in this direction is now 30 × DL.

For spectral lines from the first modulator in Fig. 62.26, the modes were also dispersed to a separation of 1/2 DL in the target plane, but the number of modes (i.e., the total angular spread) was allowed to vary while keeping the bandwidth constant. The bandwidth was maintained at a value near 4 Å (IR) by varying the modulation frequency ν_1 inversely with the number of spectral lines. (This bandwidth is about 10% lower than the value used by Eimerl.) A secondary constraint—that the frequencies from the two modulators should be incommensurate—could have been imposed. However, to simplify the calculation, it was only required that ν_1 should be an odd multiple of 0.5 GHz. This approach assured that when its modes were combined with those from the 3-GHz modulator, the resultant modes would have equally spaced frequencies separated by $\delta\nu = 0.5$ GHz. (The resultant modes have frequencies composed of a harmonic from one modulator plus a harmonic from the second.) Beam smoothing will then occur for averaging times up to 2 ns $(1/\delta\nu)$, which is the time required to smooth nearest-neighbor modes. If longer smoothing times are applicable, then ν_1 can be chosen so that the resultant modes are more closely spaced in frequency.

Figure 62.28 shows the effect of increasing the angular dispersion in one direction. The rms nonuniformity for a single beam versus averaging time is plotted. Here, the rms nonuniformity is defined as the intensity fluctuation around the

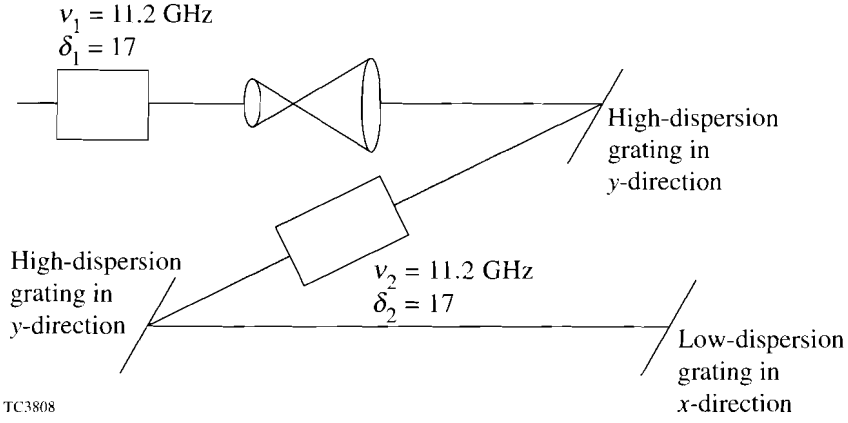

Figure 62.26
Configuration for 2-D SSD proposed for the NIF laser (Ref. 4). Here ν_1 and ν_2 are the modulation frequencies for the two modulators, and δ_1 and δ_2 are the modulation indices, corresponding to 1/2 the number of spectral modes.

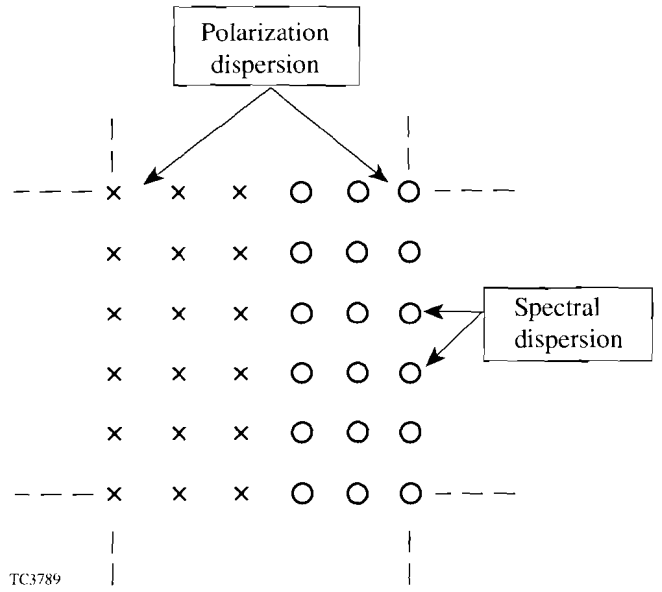

Figure 62.27
Strategy for combining 2-D SSD with polarization dispersion. The "x" and "o" positions represent the locations of the dispersed spectral modes for the two polarization components. The components should be separated by at least 1/2 of a speckle distance.

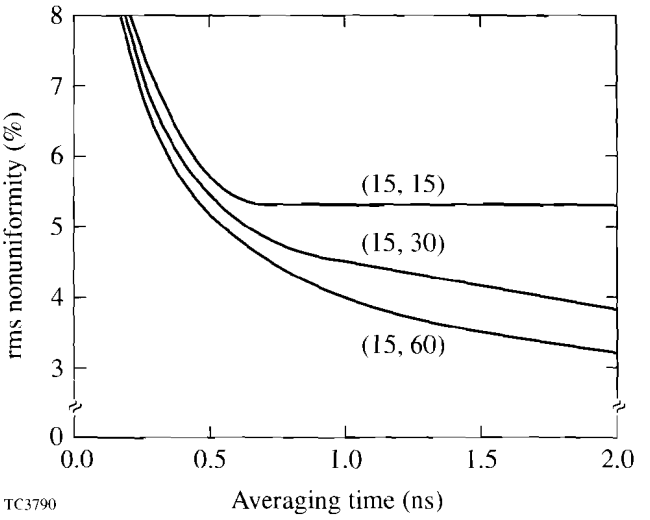

Figure 62.28
Improved irradiation nonuniformity with increased pinhole size. The numbers in parentheses indicate the angular dispersion for the two perpendicular directions, in terms of the beam's UV diffraction limit.

diffraction-limited envelope that would be produced if interference between all phase-plate elements were absent. The rms value was evaluated at the center of the beam, over a square region given by ±0.1 times the target radius in each direction. This gives a good sampling of the short-wavelength structure. (Long-wavelength nonuniformity is more appropriately discussed in conjunction with the effects of multiple-beam overlap.) The three curves in Fig. 62.28 are labeled by the angular deflection (in terms of the beam's UV diffraction limit) in each direction.

The single-beam results in Fig. 62.28 show that if we are interested only in averaging times less than ~500 ps, then there is little advantage to increasing the angular dispersion. However, if averaging times of ~1 ns or larger are relevant, then substantial improvements in uniformity can be achieved from increased dispersion. The majority of the effect is achieved at 30 × DL: For a 2-ns averaging time, the rms nonuniformity is reduced by 40%, compared with the 15 × DL result. (For 60 × DL, the reduction is increased to 65%.) The improved uniformity is probably the result of smoothing some of the longer-wavelength nonuniformities that become accessible with increased angular dispersion. (All three cases in Fig. 62.28 use the same bandwidth.) Table 62.III summarizes some of the SSD parameters and results.

The uniformity results for spherical illumination, using multiple beam overlap, are shown in Fig. 62.29, which uses the configuration of 48 clusters of 4 beams from Table 62.II with the pointing correction for the polar ring of beams. The axes of the beams in each cluster were also shifted by 20% of the target radius (using wedges) to produce an intensity envelope for the cluster that was less center-peaked than for the individual beams. (This could also be accomplished by using the phase plate to shape the envelope.) The beams were mapped directly onto the target surface, and the nonuniformity was expressed in terms of spherical harmonics for modes up to 512. No refractive smoothing or thermal smoothing in a plasma atmosphere was used, except indirectly by neglecting the very-short-wavelength structure with spherical harmonic modes greater than 512. Interference between the beams was not included in the calculation. This is justified for the interference between beams within a cluster and between beams from different clusters with different frequencies, as this structure will smooth within ~5 ps. Interference between beams (of the same frequency) from different clusters was not considered because this nonuniformity has spatial wavelengths that are much shorter than the minimum considered here. Such very-short-wavelength nonuniformity would be smoothed by thermal conduction within the target, over distances of only a few microns.

Table 62.III: Parameters related to the large-bandwidth modulator and the resultant single-beam rms nonuniformity.

	Total Angular Dispersion (DL)		
	15	30	60
Modulation frequency (GHz)	13.50	6.5	3.5
Bandwidth (Å, IR)	4.05	3.9	4.2
Single-beam nonuniformity			
Δt = 500 ps	5.9%	5.7%	5.4%
Δt = 2 ns	5.3%	3.9%	3.3%

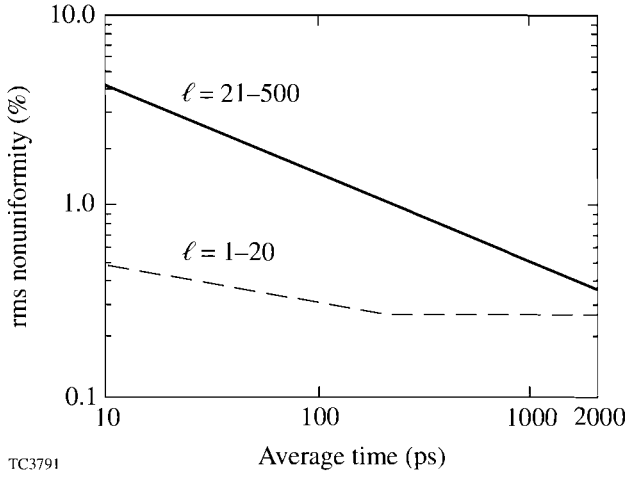

Figure 62.29
Irradiation nonuniformity for spherical irradiation as a function of averaging time. The ℓ values indicate the spherical harmonic modes for the two curves shown.

The nonuniformity for spherical irradiation (Fig. 62.29) has been separated into a long-wavelength component, with spherical harmonic modes $\ell \leq 20$, and a shorter-wavelength component with $21 \leq \ell \leq 512$. The long-wavelength modes are relatively static and are dominated by the shape of the cluster intensity envelope and the number of clusters. It is possible that this component of nonuniformity could be further reduced by modifying the envelope shape as part of the phase-plate design. The shorter-wavelength modes (21–512) decrease with averaging time t roughly as $t^{-1/2}$. This is the same scaling as ISI[9] and is obtained from the superposition of different random speckle patterns.

Finally, it should be pointed out that there is still additional nonuniformity present, with $\ell > 512$, from structure in the individual beams. As an example, Fig. 62.30 shows the modal decomposition for an averaging time of 2 ns. The nonuniformity clearly extends even above 512. The largest mode number that should be present can be estimated as follows: The largest mode ℓ_{max} is related to the wavelength of the smallest structure $\delta\lambda$ and to the target diameter by

$$\ell_{max} = \pi D/\delta\lambda .$$

The smallest wavelength should correspond roughly to the beam's diffraction limit (i.e., one speckle). Since D is 250 times larger for this calculation, we have $\ell_{max} \sim 800$. It remains to be determined what effect the very-short-wavelength structure has on target performance.

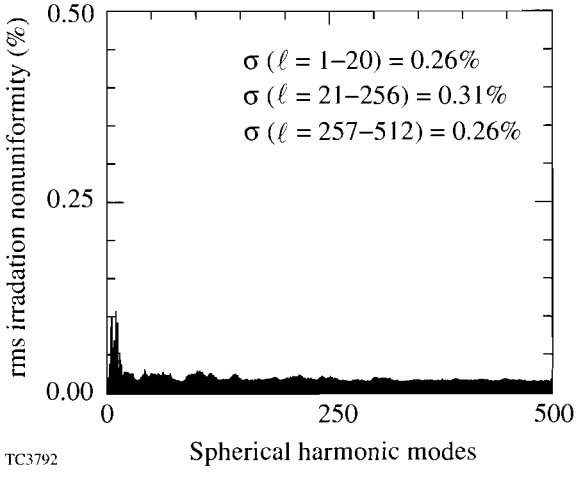

Figure 62.30
Spherical harmonic decomposition of the nonuniformity from Fig. 62.29 for 2-ns averaging time.

Summary

The NIF can produce highly uniform irradiation for direct-drive experiments if one-half of the beams are redirected to new ports closer to the "equator" of the target chamber and if 2-D SSD is implemented with polarization dispersion. The tolerances for energy imbalance among the beams, beam mispointing, and errors in target positioning depend on how much long-wavelength nonuniformity (spherical harmonic modes 1–4) the target can accept without serious degradation in performance. Using 1% for the maximum nonuniformity in these modes, we have the following constraints: (1) energy imbalance among the beams should be less than ~5%; (2) cluster mispointing should not exceed ~5% of the target radius; and (3) the target positioning error should be less than ~2% of the target radius.

The optimal pinhole size for SSD is another issue that depends on the target design. If intensity-averaging times greater than ~1 ns are of interest, then there is a definite advantage for the pinhole to be able to accommodate a divergence of $30 \times$ DL in one direction and $15 \times$ DL in the other for UV irradiation. It would be useful to determine what effect this would have on laser performance. If these divergences are available, it might be possible to optimize target designs to take advantage of the resultant higher uniformity for longer smoothing times.

ACKNOWLEDGMENT

This work was supported by the U.S. Department of Energy Office of Inertial Confinement Fusion under Cooperative Agreement No. DE-FC03-92SF19460, the University of Rochester, and the New York State Energy Research and Development Authority. The support of DOE does not constitute an endorsement by DOE of the views expressed in this article.

REFERENCES

1. S. Skupsky, R. W. Short, T. Kessler, R. S. Craxton, S. Letzring, and J. M. Soures, J. Appl. Phys. **66**, 3456 (1989).
2. J. W.-K. Mark, Phys. Lett. **114A**, 458 (1986).
3. D. Eimerl (private communication).
4. D. Eimerl, presented at the 5th Meeting of the Inertial Confinement Fusion Advisory Committee/Defense Programs (ICFAC/DP), University of Rochester, Rochester, NY, 18–20 May 1994.
5. T. J. Kessler, Y. Lin, J. J. Armstrong, and B. Velazquez, in *Laser Coherence Control: Technology and Applications*, edited by H. T. Powell and T. J. Kessler (SPIE, Bellingham, WA, 1993), Vol. 1870, pp. 95–104.
6. S. N. Dixit *et al.*, Opt. Lett. **19**, 417 (1994).
7. Laboratory for Laser Energetics LLE Review **45**, NTIS document No. DOE/DP40200-149, 1990 (unpublished), p. 1.
8. S. N. Dixit (private communication); also J. W. Goodman in *Laser Speckle and Related Phenomena*, Topics in Applied Physics, Vol. 9, edited by J. C. Dainty (Springer-Verlag, Berlin, 1984), Chap. 2, pp. 9–75.
9. R. H. Lehmberg, A. J. Schmitt, and S. E. Bodner, J. Appl. Phys. **62**, 2680 (1987).